

# Diphoton decays of stoponium at the Large Hadron Collider

Stephen P. Martin

*Department of Physics, Northern Illinois University, DeKalb IL 60115 and  
Fermi National Accelerator Laboratory, P.O. Box 500, Batavia IL 60510*

If the lighter top squark has no kinematically allowed two-body decays that conserve flavor, then it will form hadronic bound states. This is required in models that are motivated by the supersymmetric little hierarchy problem and obtain the correct thermal relic abundance of dark matter by top-squark-mediated neutralino annihilations, or by top-squark-neutralino co-annihilations. It is also found in models that can accommodate electroweak-scale baryogenesis within minimal supersymmetry. I study the prospects for detecting scalar stoponium from its diphoton decay mode at the Large Hadron Collider, updating and correcting previous work. Under favorable circumstances, this signal will be observable over background, enabling a uniquely precise measurement of the superpartner masses through a narrow peak in the diphoton invariant mass spectrum, limited by statistics and electromagnetic calorimeter resolutions.

## Contents

<b>I. Introduction</b>	2
<b>II. Diphoton signal for stoponium and backgrounds</b>	3
<b>III. Results for compressed supersymmetry models</b>	8
<b>IV. Results for models with electroweak-scale baryogenesis</b>	12
<b>V. Outlook</b>	14
<b>Appendix: Stoponium partial decay widths</b>	14
<b>References</b>	16

## I. INTRODUCTION

The classic collider signatures for supersymmetry depend on the presence of missing energy carried away by a stable, neutral, weakly interacting lightest supersymmetric particle in each event. (For reviews, see [1, 2, 3]. This paper follows the conventions and notations of the last reference.) In a sense, this is disappointing, because there are no kinematic mass peaks whose positions would yield measurements of superpartner masses. Observables at hadron colliders can give precision determinations of superpartner mass differences by way of kinematic edges and other distributions, but if  $R$ -parity is conserved the overall mass scale will be much harder to ascertain with precision in most models [4, 5].

A possible exception occurs if the supersymmetric particles can form resonances that annihilate into final states containing only Standard Model particles with strong or electromagnetic interactions. An example is stoponium, a bound state of a pair of top squarks. The lighter top squark (or stop)  $\tilde{t}_1$  has possible flavor-preserving two-body decays into the lightest chargino or neutralino,

$$\tilde{t}_1 \rightarrow b\tilde{C}_1, \quad (1.1)$$

$$\tilde{t}_1 \rightarrow t\tilde{N}_1, \quad (1.2)$$

which, if kinematically allowed, would cause it to decay long before it could form a hadronic bound state. However, the first decay will be closed if the chargino  $\tilde{C}_1$  is not at least 5 GeV lighter than the top squark, and the large top quark mass means that the second decay may well also be kinematically closed. In most of the so-called mSUGRA parameter space, this situation is not encountered, but it is nevertheless quite possible and even common in other model frameworks. Then one must consider three-body (and four-body) decays that preserve flavor, and a two-body decay to charm that violates flavor:

$$\tilde{t}_1 \rightarrow W^{(*)}b\tilde{N}_1, \quad (1.3)$$

$$\tilde{t}_1 \rightarrow c\tilde{N}_1. \quad (1.4)$$

The partial widths associated with the decays (1.3) and (1.4) are known [6, 7] to be far smaller than the binding energy of stoponium or other bound hadronic states involving  $\tilde{t}_1$ .

Therefore, it is worthwhile on general grounds to consider signals for the production and decay of stoponium. At hadron colliders, stoponium is produced primarily in gluon-gluon fusion, with the largest cross-section for the  $1S$  ( $J^{PC} = 0^{++}$ ) scalar ground state, denoted in the following as  $\eta_{\tilde{t}}$ . This state will decay primarily by annihilation, with the possible two-body final states including  $gg$ ,  $\gamma\gamma$ ,  $W^+W^-$ ,  $ZZ$ ,  $h^0h^0$ ,  $t\bar{t}$ ,  $b\bar{b}$ , and  $\tilde{N}_1\tilde{N}_1$ . The QCD backgrounds for the gluon and quark final states are too huge to contemplate a signal. Also, the  $W^+W^-$ ,  $ZZ$ , and  $h^0h^0$  final states are plagued by either large backgrounds or small branching fractions, and the  $\tilde{N}_1\tilde{N}_1$  final state does not give a reconstructable signature. However, Drees and Nojiri in [8, 9] pointed out that  $\eta_{\tilde{t}} \rightarrow \gamma\gamma$  provides a viable signal at the CERN Large Hadron Collider. (See also refs. [10]-[14] for earlier works related to stoponium at hadron colliders.)

Refs. [8, 9] appeared before two important experimental developments which bring this possibility into sharper focus. The first is the 1995 discovery of the top quark. Second, the results of WMAP and other experiments have bracketed the density of cold dark matter in the standard cos-

mology [15]-[17]. This is important because the measurement of  $\Omega_{\text{DM}}h^2 \approx 0.11$  can be correlated with a top squark light enough to forbid the decays (1.1) and (1.2) in at least two scenarios. First, neutralino LSP and top-squark co-annihilations can give the observed dark matter density if the mass difference  $m_{\tilde{t}_1} - m_{\tilde{N}_1}$  is in a small range [18]-[22]. Second, the neutralino LSP can efficiently pair-annihilate into a top-anti-top pair, mediated by the  $t$ -channel exchange of a top squark that is not more than about 100 GeV heavier than the LSP [23, 24]. These two scenarios are often continuously connected in parameter space, but the latter one requires far less fine adjustment of parameters to realize. It does, however, require that the gaugino masses are not unified in the way assumed in mSUGRA models. A particularly attractive model framework that meets the requirements of the stop-mediated annihilation scenario is provided by “compressed supersymmetry” [23, 24], in which the gluino mass parameter is taken to be significantly smaller than the wino mass parameter at the scale of apparent gauge coupling unification  $M_{\text{GUT}} \approx 2 \times 10^{16}$  GeV. A reduction of the gluino mass compared to the wino and bino mass parameters can also ameliorate [25] the supersymmetric little hierarchy problem. Another quite different motivation for a light top squark is provided by models that can have a strongly first-order phase transition leading to electroweak-scale baryogenesis [26]-[28]; this can also incorporate the neutralino-stop co-annihilation scenario for dark matter.

In this paper, I will consider the  $\eta_{\tilde{t}} \rightarrow \gamma\gamma$  signal at the LHC along similar lines to ref. [9], taking into account the now known top-quark mass, considering motivated models that agree with the observed dark matter density and Higgs mass constraints, and using a more liberal angular cut but a more conservative energy resolution for the electromagnetic calorimeter. I also correct (see Appendix) factor of 2 errors appearing in the  $gg$  and  $\gamma\gamma$  partial decay widths in ref. [9]. This leads to a somewhat more pessimistic evaluation of the detection potential, but in many parts of parameter space the diphoton signal will be detectable given a large integrated luminosity at the LHC.

## II. DIPHOTON SIGNAL FOR STOPONIUM AND BACKGROUNDS

The leading-order partial decay widths of  $\eta_{\tilde{t}}$  into gluon and photon final states are:

$$\Gamma(\eta_{\tilde{t}} \rightarrow gg) = \frac{4}{3}\alpha_S^2 |R(0)|^2 / m_{\eta_{\tilde{t}}}^2, \quad (2.1)$$

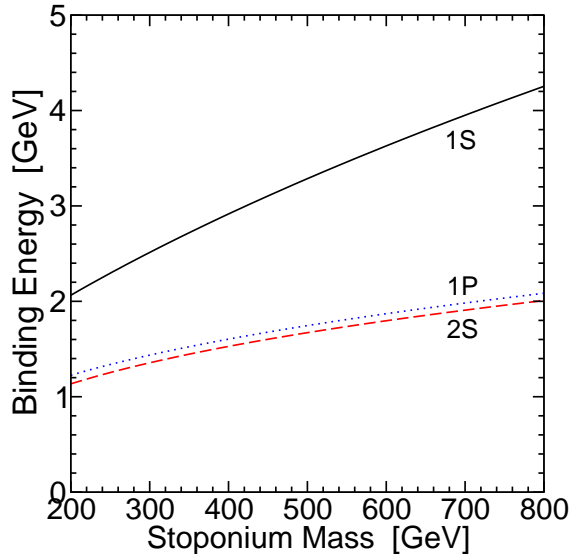
$$\Gamma(\eta_{\tilde{t}} \rightarrow \gamma\gamma) = \frac{32}{27}\alpha^2 |R(0)|^2 / m_{\eta_{\tilde{t}}}^2, \quad (2.2)$$

where  $R(0) = \sqrt{4\pi}\psi(0)$  is the radial wavefunction at the origin. In the Coulomb approximation to the bound state problem,  $|R(0)|^2 / m_{\eta_{\tilde{t}}}^2 = 4\alpha_S^3 m_{\eta_{\tilde{t}}} / 27$ . However, the study of ref. [29] indicates a softer potential, with the Coulomb limit not obtained even for very large bound state masses. In the following, I will adopt the  $\Lambda_{\overline{\text{MS}}}^{(4)} = 300$  MeV parameterizations of the wavefunction at the origin and the binding energy as given in ref. [29]:

$$|R(0)|^2 / m_{\eta_{\tilde{t}}}^2 = (0.1290 + 0.0754L + 0.0199L^2 + 0.0010L^3) \text{ GeV}, \quad (2.3)$$

$$2m_{\tilde{t}_1} - m_{\eta_{\tilde{t}}} = (3.274 + 1.777L + 0.560L^2 + 0.081L^3) \text{ GeV}, \quad (2.4)$$

FIG. 1: The binding energies for the 1S, 2S, and 1P stoponium states as a function of the stoponium mass, as computed from the potential model of ref. [29] with  $\Lambda_{\overline{\text{MS}}}^{(4)} = 300$  MeV.



where  $L = \ln(m_{\tilde{t}_1}/250 \text{ GeV})$ . The binding energies of the 1S ground state and the 2S and 1P excited states are shown in Figure 1. It should be noted that these results are based on a considerable extrapolation from known experimental results on  $c\bar{c}$  and  $b\bar{b}$  bound states, and other potentials can give quite different results. (For example, see the ones reviewed in ref. [30].) The partial width into gluons is of order 2 MeV over the considered range of  $m_{\eta_{\tilde{t}}}$ . The fact that the binding energy is much larger shows that the stoponium bound state will indeed form, provided that other partial widths do not overwhelm  $\Gamma(\eta_{\tilde{t}} \rightarrow gg)$  by a factor of 1000, a requirement easily satisfied by models studied below.

At leading order and in the narrow-width approximation, the production cross-section for  $\eta_{\tilde{t}}$  in  $pp$  collisions is given in terms of its gluonic decay width by

$$\sigma(pp \rightarrow \eta_{\tilde{t}}) = \frac{\pi^2}{8m_{\eta_{\tilde{t}}}^3} \Gamma(\eta_{\tilde{t}} \rightarrow gg) \int_{\tau}^1 dx \frac{\tau}{x} g(x, Q^2) g(\tau/x, Q^2), \quad (2.5)$$

where  $g(x, Q^2)$  is the gluon parton distribution function, and  $\tau = m_{\eta_{\tilde{t}}}^2/s$  in terms of the  $pp$  collision energy squared  $s$ . In the following, I use the CTEQ5L [31] set for the parton distribution functions, evaluated at  $Q = m_{\eta_{\tilde{t}}}$  for the signal and  $Q = M_{\gamma\gamma}$  for the backgrounds.

For comparison, the ratio of the stoponium production cross-section to that of a Standard Model Higgs boson  $H$  with the same mass is just  $\sigma(pp \rightarrow \eta_{\tilde{t}})/\sigma(pp \rightarrow H) = \Gamma(\eta_{\tilde{t}} \rightarrow gg)/\Gamma(H \rightarrow gg)$  at leading order. For  $m_{\eta_{\tilde{t}}} = (200, 250, 300, 400, 500, 600, 700, 800)$  GeV, this is approximately  $\sigma(pp \rightarrow \eta_{\tilde{t}})/\sigma(pp \rightarrow H) = (1.44, 0.74, 0.40, 0.098, 0.064, 0.054, 0.050, 0.048)$ . However,  $\text{BR}(\eta_{\tilde{t}} \rightarrow \gamma\gamma)$  is much larger than  $\text{BR}(H \rightarrow \gamma\gamma)$  for masses larger than 140 GeV, because the latter is loop-suppressed compared to relatively huge widths into  $ZZ^{(*)}$ ,  $WW^{(*)}$ , and  $t\bar{t}$  final states. This explains why the stoponium signal  $\eta_{\tilde{t}} \rightarrow \gamma\gamma$  can be viable over the mass range where  $H \rightarrow \gamma\gamma$  observation is not possible. In contrast,  $\text{BR}(\eta_{\tilde{t}} \rightarrow ZZ)/\text{BR}(H \rightarrow ZZ)$  turns out to be at most about 0.3 over the same mass range. This explains why the search for stoponium in  $pp \rightarrow \eta_{\tilde{t}} \rightarrow ZZ$  in the  $\ell^+\ell^-\ell'^+\ell'^-$  and  $\ell^+\ell^-\nu\bar{\nu}$  channels is almost certainly not viable [9] for masses where it is the best search option for  $H$ .

Now, multiplying eq. (2.5) by the branching fraction into a diphoton state, and rearranging the

factors, one obtains:

$$\sigma(pp \rightarrow \eta_{\bar{i}} \rightarrow \gamma\gamma) = \frac{\pi^2}{8m_{\eta_{\bar{i}}}^3} \text{BR}(\eta_{\bar{i}} \rightarrow gg) \Gamma(\eta_{\bar{i}} \rightarrow \gamma\gamma) \int_{\tau}^1 dx \frac{\tau}{x} g(x, Q^2) g(\tau/x, Q^2). \quad (2.6)$$

This way of writing the result is useful because, in many realistic models, the gluonic decay dominates over all other final states. Therefore, it is instructive to adopt an idealized limit where  $\text{BR}(\eta_{\bar{i}} \rightarrow gg) \approx 1$  as a standard reference scenario. (Note that the  $\gamma\gamma$  partial width is typically about 0.005 of the  $gg$  partial width.) Then results for particular models can be obtained by scaling the signal cross-section by the actual  $\text{BR}(\eta_{\bar{i}} \rightarrow gg)$ .

We next consider the diphoton backgrounds at the LHC. The  $pp \rightarrow \gamma\gamma$  process has parton-level contributions:

$$q\bar{q} \rightarrow \gamma\gamma, \quad (2.7)$$

$$gg \rightarrow \gamma\gamma, \quad (2.8)$$

with leading-order differential cross-sections found in [32]-[35]. The leading order total cross-section for eq. (2.7) is proportional to  $\ln[(1+z_0)/(1-z_0)] - z_0$ , where  $z_0$  is the cut on  $|\cos\theta_*|$ , with  $\theta_*$  the photon momentum angle with respect to the beam direction in the center-of-momentum frame. Since the signal is isotropic, with a total signal cross-section proportional to  $z_0$ , it follows that  $S/\sqrt{B}$  is maximized for  $z_0 \approx 0.705$ . The process (2.8) involves Feynman diagrams that have quark box loops. It is somewhat more central than the  $q\bar{q}$  background, and so would favor a larger cut  $z_0$ , but it is quite subdominant over the diphoton mass range considered here. For simplicity, I will impose a cut on both signal and background of

$$|\cos\theta_*| < 0.7 \quad (2.9)$$

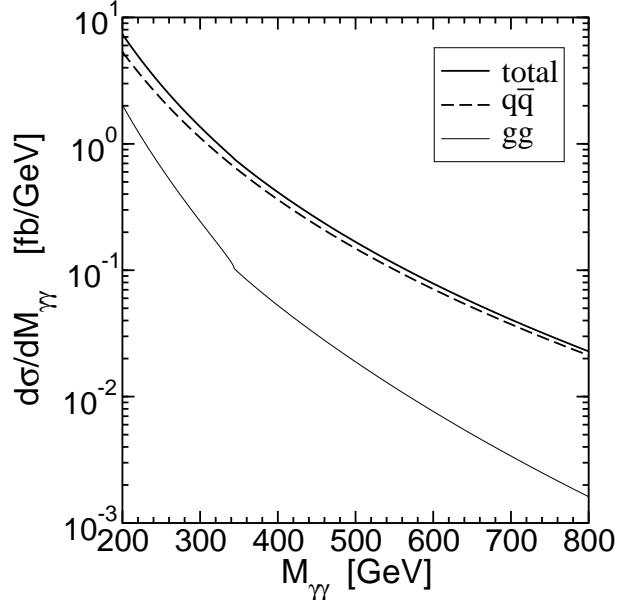
in the center-of-momentum frame. This guarantees a high  $p_T$  for the photons, for high-mass stoponium states. In addition, I will require that the photons be well-separated from the beam direction and the remnant beam jets, so

$$|\cos\theta| < 0.95 \quad (2.10)$$

(or  $|\eta| < 1.83$ ) in the lab frame. The cut (2.9) is apposite for low rapidities, and (2.10) for high rapidities. The results for the background at leading order after these cuts are shown in fig. 2 as a function of the invariant mass of the diphoton system,  $M_{\gamma\gamma}$ .

Higher-order corrections to the background can be quite important, increasing the cross-section after cuts by a factor of 2 or more [36]-[39]. This includes a large contribution from the hard scattering process  $qg \rightarrow \gamma\gamma q$  (and  $\bar{q}g \rightarrow \gamma\gamma\bar{q}$ ) and the related process  $qg \rightarrow \gamma q$  followed by a photon from the fragmentation of the quark jet, as well as from double fragmentation contributions. Imposing isolation cuts on hadronic activity near the photons and requiring the absence of additional hard jets reduces these backgrounds considerably. The isolation cut requirement is necessary anyway, to eliminate an otherwise large background from jets faking photons, including  $\pi^0$  and  $\eta$  decays that are not resolved in the electromagnetic calorimeter. Also, the initial-state gluon contribu-

FIG. 2: The differential cross-section  $d\sigma/dM_{\gamma\gamma}$  for the diphoton backgrounds in  $pp$  collisions at  $\sqrt{s} = 14$  TeV, due to the parton-level processes  $q\bar{q} \rightarrow \gamma\gamma$  and  $gg \rightarrow \gamma\gamma$ , at leading order. Here  $M_{\gamma\gamma}$  is the diphoton invariant mass. The cuts imposed on the angle with respect to the beam axis are  $|\cos\theta_*| < 0.7$  in the diphoton center-of-momentum frame and  $|\cos\theta| < 0.95$  in the lab frame. The kink in the  $gg$  background at  $M_{\gamma\gamma} = 2m_t$  is due to the threshold in the top-quark box loop.



tions are not as important in the present case as in the well-studied Standard Model Higgs signal mass range  $m_H < 140$  GeV, because the gluon parton distribution function is relatively smaller at larger  $x$ . The background contributions from jets without charged tracks faking photons can likely be reduced to a small level with isolation cuts imposed in offline analysis [40]. In any case, because the stoponium diphoton resonance will be very narrow, in practice the background should be determined directly from LHC data by a sideband analysis.

Inclusion of the higher-order background contributions is beyond the scope of this paper, especially since the corresponding higher-order corrections to the stoponium signal cross-section are not available. In addition, the increased background will likely be at least partly compensated for by contributions to the signal from production of excited stoponium states, followed either by decays to the  $1S$   $\eta_{\bar{t}}$  state by emission of photons or soft mesons or by direct decays to  $\gamma\gamma$  [9]. For example, the  $2S$  state has a binding energy that is probably only slightly less than the  $1P$  state (see fig. 1), so decays of  $2S$  stoponium to the  $1P$  state and a meson would be kinematically forbidden according to this potential model. The  $2S$  non-annihilation decays therefore will most likely go entirely to the  $1S$  ground state. These signal contributions will be effectively merged due to the detector energy resolution, leading to an overall enhancement of the signal of perhaps a factor of 1.5 (see fig. 9 of ref. [9]). This unknown enhancement is not included here, to be conservative.

The energy resolutions of the ATLAS and CMS electromagnetic calorimeters at the LHC will clearly dominate over the very small intrinsic width of stoponium in determining the experimental width of the signal peak. Therefore, to estimate the significance of the signal over the background, I consider a bin with width  $0.04m_{\eta_{\bar{t}}}$ , chosen to contain essentially all of the signal peak on which it is centered. (See ref. [40] for a CMS study of a similar diphoton signal peak at higher masses, and the CMS and ATLAS physics technical design reports [4, 5] for estimates that put the electromagnetic calorimeter resolutions at roughly the per cent level.) The resulting comparison of the signal and background within such a bin is found in fig. 3. Here I have taken the signal corresponding to the idealized reference case of  $\text{BR}(\eta_{\bar{t}} \rightarrow gg) + \text{BR}(\eta_{\bar{t}} \rightarrow \gamma\gamma) = 1$ .

The resulting integrated luminosities needed to reach significances  $S/\sqrt{B} = 2, 3, 4, 5$ , taking enough events to use Gaussian statistics, are shown in fig. 4. Because there are many bin widths

FIG. 3: The  $pp \rightarrow \eta_{\tilde{t}} \rightarrow \gamma\gamma$  cross-section and the irreducible background in a bin with  $|M_{\gamma\gamma} - m_{\eta_{\tilde{t}}}| < 0.02m_{\eta_{\tilde{t}}}$ , for  $pp$  collisions at  $\sqrt{s} = 14$  TeV, as a function of the stoponium mass  $m_{\eta_{\tilde{t}}}$ . Both are computed at leading order, with the same angular cuts as in Figure 2. The signal assumes an idealized limit in which  $\text{BR}(\eta_{\tilde{t}} \rightarrow gg) + \text{BR}(\eta_{\tilde{t}} \rightarrow \gamma\gamma)$  is 100%.

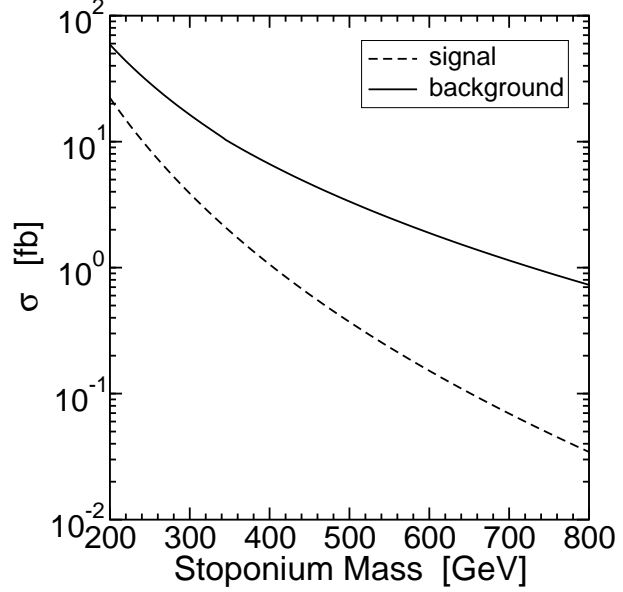
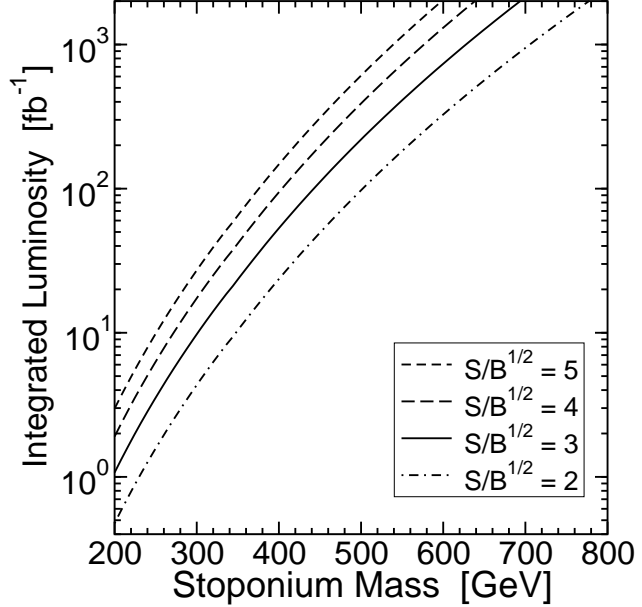


FIG. 4: Total integrated luminosity yielding an expected  $S/\sqrt{B} = 2, 3, 4, 5$  for  $M_{\gamma\gamma}$  in a bin with  $|M_{\gamma\gamma} - m_{\eta_{\tilde{t}}}| < 0.02m_{\eta_{\tilde{t}}}$ , as a function of the stoponium mass  $m_{\eta_{\tilde{t}}}$ , for  $pp$  collisions at  $\sqrt{s} = 14$  TeV, in the idealized limit that  $\text{BR}(\eta_{\tilde{t}} \rightarrow gg) + \text{BR}(\eta_{\tilde{t}} \rightarrow \gamma\gamma)$  is 100%. The integrated luminosity needed to achieve a given  $S/\sqrt{B}$  can be obtained by scaling by  $1/[\text{BR}(\eta_{\tilde{t}} \rightarrow gg)]^2$ .



over the mass range considered, the probability of a 2-sigma excess in one of them arising just from a fluctuation in the background is not negligible. However, the LHC will likely have already produced a preliminary estimate of the  $\tilde{t}_1$  mass from gluino or direct open stop production before the stoponium diphoton signal becomes feasible, so the search range for the stoponium mass peak will not be too large. The luminosities in fig. 4 should be multiplied by  $1/[\text{BR}(\eta_{\tilde{t}} \rightarrow gg)]^2$ , since the required luminosity scales like the square of the signal cross-section eq. (2.6).

From fig. 4 one sees that the expected significance for a 500 GeV stoponium resonance will be at most only about  $S/\sqrt{B} = 2$  for a canonical high luminosity year of data ( $100 \text{ fb}^{-1}$ ). This is more pessimistic than in ref. [9], due in part to a factor of 2 error in that paper in the  $\eta_{\tilde{t}} \rightarrow \gamma\gamma$  width, but also due to their assumption of electromagnetic calorimeter resolution providing an acceptable bin for  $M_{\gamma\gamma}$  that is twice as narrow as assumed in the present paper. However, a more sophisticated approach based on a maximum likelihood fit, which is beyond the scope of this paper,

will certainly do better than the simple counting in a single bin used here. (Note that the detector mass resolution will in any case be smaller than the bin width needed to catch all of the signal events.) Also, the integrated luminosity needed is proportional to the square of the signal cross-section and to the reciprocal of the background, and so is strongly dependent on assumptions that are difficult to evaluate confidently at present.

### III. RESULTS FOR COMPRESSED SUPERSYMMETRY MODELS

In the previous section, I estimated the integrated luminosity needed to achieve detection of the stoponium resonance at a given significance, but considering an idealized reference model where  $\text{BR}(\eta_{\tilde{t}} \rightarrow gg)$  was nearly 100%. In this section and the next, I consider the actual branching ratio achieved in realistic, motivated models that satisfy the dark matter density and Higgs mass constraints. As discussed in the previous section, the integrated luminosity needed for discovery scales like  $1/[\text{BR}(\eta_{\tilde{t}} \rightarrow gg)]^2$ .

First, I will follow ref. [23, 24] and consider models where the bino, wino, and gluino masses can be parameterized at  $M_{\text{GUT}}$  by:

$$M_1 = m_{1/2}(1 + C_{24}), \quad (3.1)$$

$$M_2 = m_{1/2}(1 + 3C_{24}), \quad (3.2)$$

$$M_3 = m_{1/2}(1 - 2C_{24}), \quad (3.3)$$

corresponding to an  $F$ -term source for supersymmetry breaking in a linear combination of the singlet and adjoint representations of  $SU(5)$ . For the sake of simplicity, I also assume a common scalar mass  $m_0$  and scalar trilinear coupling  $A_0$  at  $M_{\text{GUT}}$ . For  $C_{24}$  of order 0.2, one finds that the supersymmetric little hierarchy problem is ameliorated, with a significant part of parameter space where  $\tilde{t}_1$  is the next-to-lightest supersymmetric particle. The dark matter thermal relic abundance can be sufficiently suppressed by  $\tilde{N}_1 \tilde{N}_1 \rightarrow t\bar{t}$  due to  $t$ -channel  $\tilde{t}_1$  exchange, giving  $\Omega_{\text{DM}} h^2 = 0.11$  in accord with observations. I impose this as a requirement, by adjusting the value of  $m_0$  for fixed values of the other parameters, using the program `micrOMEGAs 2.0.1` [41] (checked for approximate agreement with `DarkSUSY` [42]) interfaced to the supersymmetry model parameters program `SOFTSUSY 2.0.11` [43] (checked for approximate agreement with `SuSpect` [44] and `ISAJET` [45]). The resulting  $m_0$  values are reasonably small and do not require fine-tuning. In these models,  $m_{\tilde{t}_1} - m_{\tilde{N}_1} < 100$  GeV, so that stoponium will indeed form as a bound state before it has a chance to decay.<sup>†</sup> These stop-mediated annihilation models are continuously connected in parameter space to more fine-tuned regions in which the  $\tilde{t}_1, \tilde{N}_1$  mass difference is just right to allow efficient stop-neutralino co-annihilations.

In general, as shown in ref. [9], the most important final states in competition with the  $gg$  and  $\gamma\gamma$  ones are  $W^+W^-$ ,  $ZZ$ ,  $h^0h^0$ ,  $t\bar{t}$ ,  $b\bar{b}$ , and  $\tilde{N}_1\tilde{N}_1$ . Formulas for the decay widths for these final states were given in ref. [9], and are presented in the Appendix of the present paper in a

---

<sup>†</sup> The LHC phenomenology (other than from stoponium) and dark matter detection prospects of these models have been discussed in refs. [23, 24, 46]. There has recently been considerable interest in the phenomenology of other models that achieve realistic dark matter with non-universal gaugino masses [47]-[63].



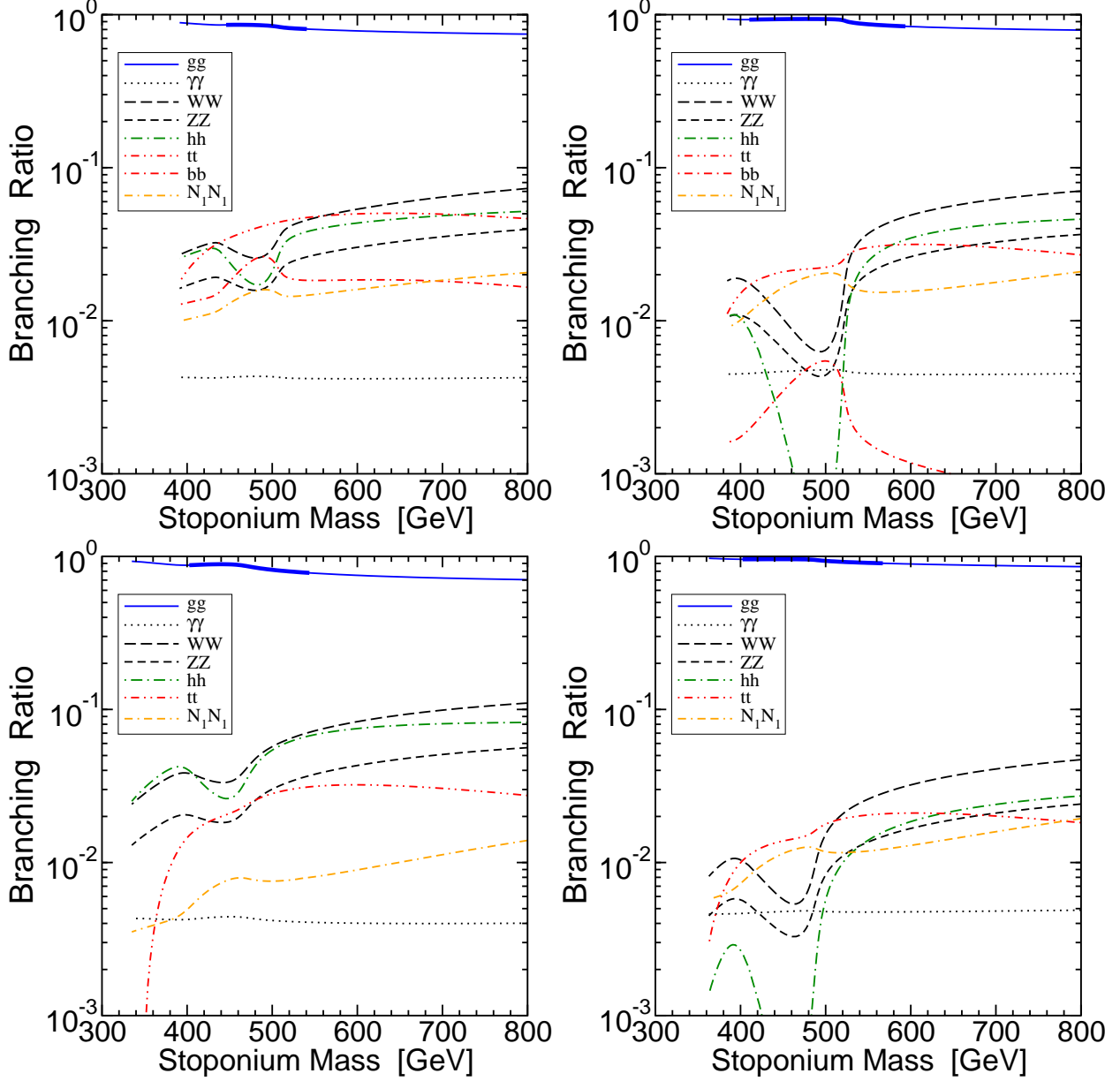


FIG. 5: The branching ratios of scalar stoponium into the most important final states, for some representative models of the type described in the text. In all cases,  $\tan\beta = 10$ ,  $\mu > 0$ , and  $M_1$  varies, with  $m_0$  adjusted to give  $\Omega_{\text{DM}}h^2 = 0.11$ . The upper left, upper right, lower left, and lower right panels have respectively  $(C_{24}, -A_0/M_1) = (0.19, 1)$ ,  $(0.21, 1)$ ,  $(0.21, 1.5)$ , and  $(0.24, 1.5)$ . The thicker part of the  $gg$  line indicates the range of stoponium mass for which stop-mediated annihilations  $\tilde{N}_1\tilde{N}_1 \rightarrow t\bar{t}$  contribute more than 50% to  $1/\Omega_{\text{DM}}h^2$ .

different notation. Results for the branching ratios in four typical model lines are shown in fig. 5. These model lines each have a continuously varying overall gaugino mass scale, parameterized by the bino mass parameter  $M_1$ , with the wino and gluino masses at  $M_{\text{GUT}}$  then given by fixed values of  $C_{24}$ , as in eqs. (3.1)-(3.3). The parameters  $\tan\beta = 10$  and  $A_0/M_1$  are fixed, and then the value of  $m_0$  is adjusted to give  $\Omega_{\text{DM}}h^2 = 0.11$ . The four representative model lines were chosen to have  $(C_{24}, -A_0/M_1) = (0.19, 1)$ ,  $(0.21, 1)$ ,  $(0.21, 1.5)$ , and  $(0.24, 1.5)$ . The tuning of  $m_0$  needed

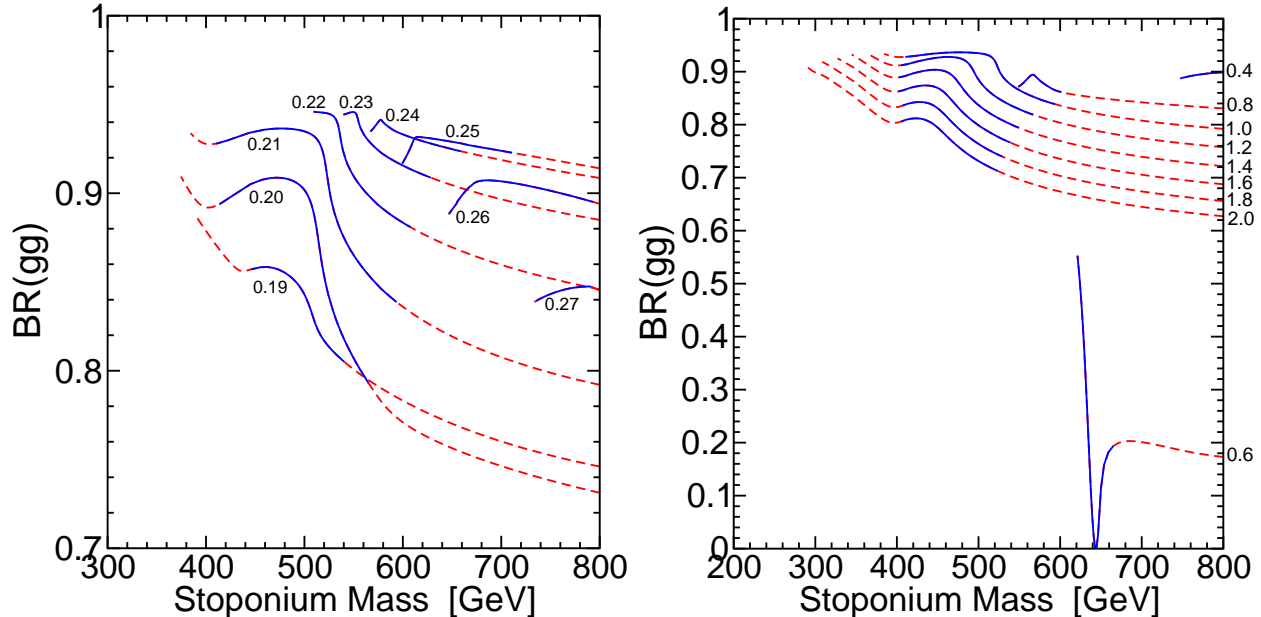


FIG. 6: The branching ratios of scalar stoponium into the  $gg$  final state, for a variety of models of the type described in the text. In the left panel,  $-A_0/M_1 = 1$  at  $M_{\text{GUT}}$ , with various  $C_{24} = 0.19$  to  $0.27$  as labeled. In the right panel,  $C_{24} = 0.21$ , with various  $-A_0/M_1 = 0.4$  to  $2.0$  as labeled on the far right. In all cases,  $\tan\beta = 10$ ,  $\mu > 0$ , and  $M_1$  varies, with  $m_0$  adjusted to give  $\Omega_{\text{DM}}h^2 = 0.11$ . The models for which stop-mediated annihilations  $\tilde{N}_1\tilde{N}_1 \rightarrow t\bar{t}$  contribute more than 50% to  $1/\Omega_{\text{DM}}h^2$  are denoted by solid (blue) lines, other models by dashed (red) lines. The integrated luminosity needed to achieve a given  $S/\sqrt{B}$  can be obtained from fig. 4 by scaling by  $1/[\text{BR}(\eta_{\tilde{t}} \rightarrow gg)]^2$ .

is particularly mild in the regions indicated by the thicker solid (blue) lines for  $\text{BR}(\eta_{\tilde{t}} \rightarrow gg)$ , corresponding to models for which  $\tilde{N}_1\tilde{N}_1 \rightarrow t\bar{t}$  dominates the annihilation of dark matter in the early universe. This typically gives  $m_{\eta_{\tilde{t}}}$  in the range 400-600 GeV. The model lines in fig. 5 show the common features that  $\text{BR}(\eta_{\tilde{t}} \rightarrow gg)$  is quite high, typically 80% or higher for the range shown, and often in excess of 90% for smaller  $m_{\eta_{\tilde{t}}}$  and smaller top-squark mixing. In the mass range where neutralino annihilation dominates, the branching ratios for  $W^+W^-$ ,  $ZZ$ , and  $h^0h^0$  final states have a welcome dip, due to destructive interferences in the amplitudes for each of these final states. The dominance of the  $gg$  final state yields branching ratio to photons that are fairly constant, between 0.004 and 0.005 over the relevant range of stoponium masses. Here and in the plots to follow, the lower endpoint on the model lines is set by the CERN LEP2 constraint on the Higgs mass, taken here to be  $m_{h^0} > 113$  GeV due to the theoretical errors in the computation.

The crucial branching ratio into the  $gg$  final state is shown in fig. 6 for different slices through parameter space. In the left panel,  $-A_0/M_1 = 1$  is held fixed and  $C_{24}$  is varied over the range 0.19 to 0.27 for which the stop-mediated neutralino annihilation to top quarks mechanism works efficiently, with  $m_0$  always adjusted to give the observed dark matter density, and  $\tan\beta = 10$  and  $\mu > 0$ . Here  $\text{BR}(\eta_{\tilde{t}} \rightarrow gg)$  is always high, but for larger  $C_{24}$ , the stoponium mass is forced up by the LEP Higgs mass bound and will be difficult or impossible to observe at LHC for  $C_{24} \gtrsim 0.26$ .

In the right panel of fig. 6, we instead fix  $C_{24} = 0.21$ , and vary  $-A_0/M_1$  in the range from 0.4 to 2.0. The  $\text{BR}(\eta_{\tilde{t}} \rightarrow gg)$  tends to decrease slightly for larger  $-A_0/M_1$  (as the top-squark mixing increases), leading to enhanced branching ratios into  $W^+W^-$ ,  $ZZ$ , and  $h^0h^0$ . However, the most dramatic effect is seen in the  $-A_0/M_1 = 0.6$  case, where the  $\text{BR}(\eta_{\tilde{t}} \rightarrow gg)$  becomes extremely small,

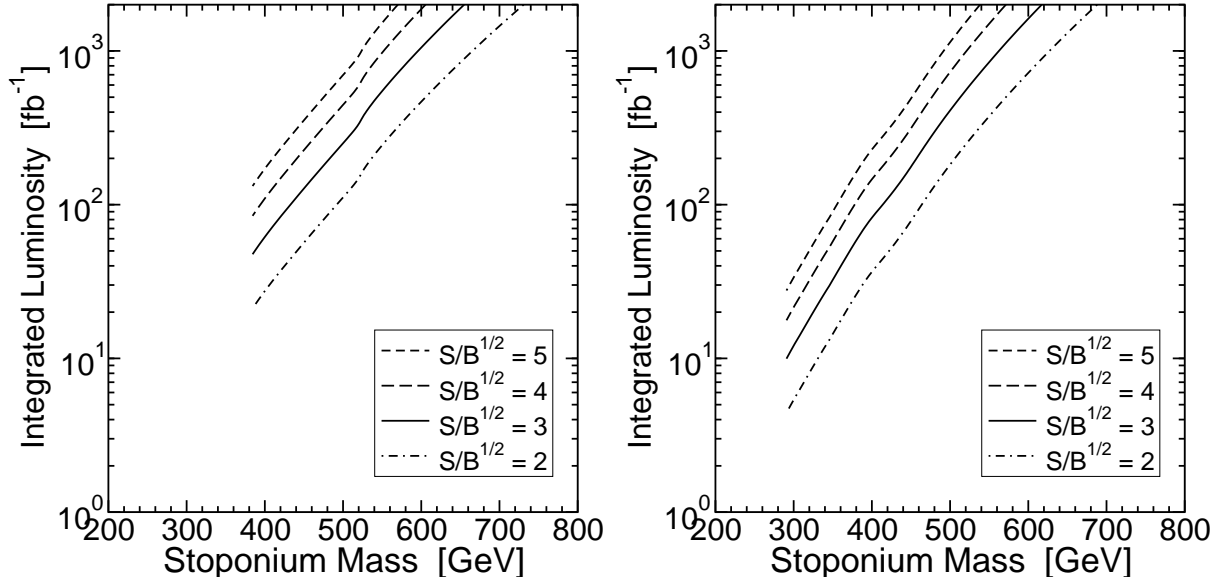


FIG. 7: Total integrated luminosity yielding an expected  $S/\sqrt{B} = 2, 3, 4, 5$  for  $M_{\gamma\gamma}$  in a bin with  $|M_{\gamma\gamma} - m_{\eta_{\tilde{t}}}| < 0.02m_{\eta_{\tilde{t}}}$ , as a function of the stoponium mass  $m_{\eta_{\tilde{t}}}$ , for  $pp$  collisions at  $\sqrt{s} = 14$  TeV, for compressed supersymmetry model lines of the type discussed in the text, with  $C_{24} = 0.21$  and  $A_0/M_1 = -1$  (left panel) and  $A_0/M_1 = -2$  (right panel).

due to the effect noted in ref. [9] of an  $s$ -channel resonance in stoponium annihilation to  $b\bar{b}$  and  $t\bar{t}$  from  $H^0$  exchange. This can ruin the possibility of stoponium detection at the LHC. In the model framework with a common fixed  $m_0$  and other values of  $C_{24}$ , this resonant annihilation to quarks occurs for a range of  $-A_0/M_1$  less than 1. It is interesting that these models correspond to the more optimistic projected sensitivity for the direct detection of dark matter in the next generation of low-background underground experiments [24]. However, more generally, the heavy neutral Higgs boson mass can be made essentially arbitrary without changing the other essential features of the model, by assuming non-universal scalar masses at  $M_{\text{GUT}}$ . Therefore, it is impossible to make any definitive statements about the complementarity of the detectability of the stoponium resonance at LHC and the direction detection of dark matter.

Another dangerous decay mode is the  $h^0h^0$  final state, which can dominate over all others if  $\eta_{\tilde{t}} \rightarrow h^0h^0$  is not too far above threshold, as noted in refs. [9, 13]. In the dark-matter-motivated models I have studied here, this turns out never to be a fatal problem, because the stoponium mass is always sufficiently large. This is illustrated in fig. 7, which shows the luminosity needed to obtain an expected  $S/\sqrt{B} = 2, 3, 4, 5$  for  $M_{\gamma\gamma}$  in a bin with  $|M_{\gamma\gamma} - m_{\eta_{\tilde{t}}}| < 0.02m_{\eta_{\tilde{t}}}$ , as a function of  $m_{\eta_{\tilde{t}}}$ , for two representative model lines with  $C_{24} = 0.21$  and  $A_0/M_1 = -1, -2$ . If the stoponium mass is small enough, detection might even occur with less than  $10 \text{ fb}^{-1}$  of data. In general, the models that are consistent with the dark matter scenario proposed in [23, 24] can be prime candidates for stoponium detection in the diphoton mode, provided that the stoponium mass is not too large and not so close to  $m_{H^0}$  as to allow a near-resonant annihilation decay.

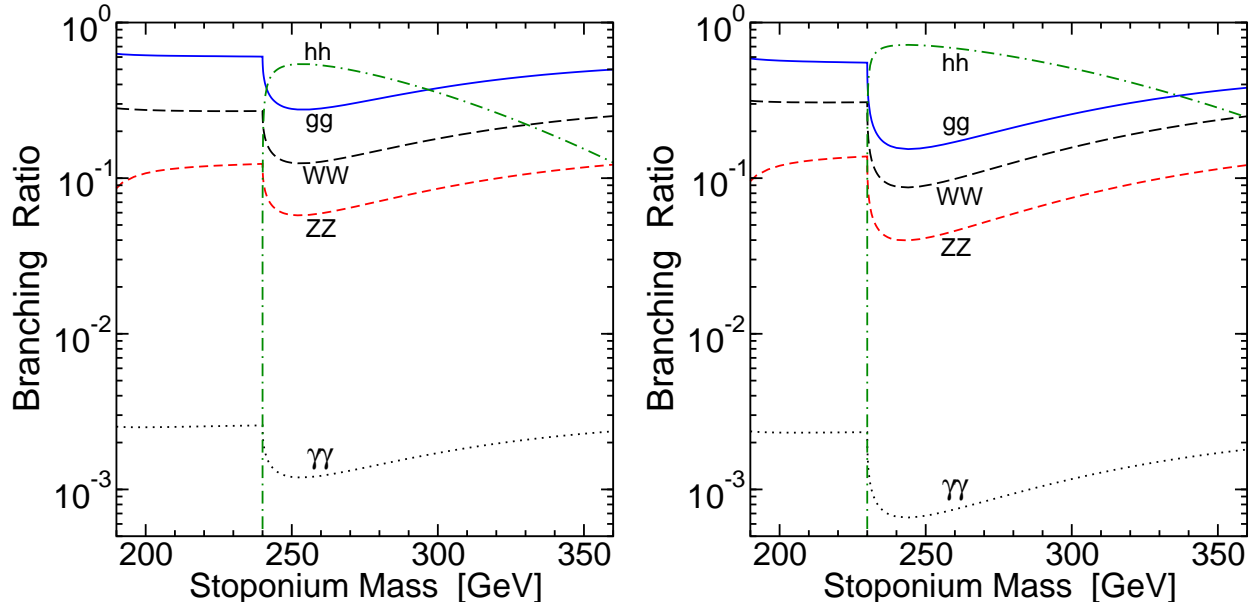


FIG. 8: The branching ratios of scalar stoponium into  $gg$ ,  $\gamma\gamma$ ,  $W^+W^-$ ,  $ZZ$ , and  $h^0h^0$  final states, for model lines motivated by electroweak-scale baryogenesis, as described in the text, with varying  $m_{\tilde{t}_1}$ . The left panel depicts a relatively optimistic case with  $m_{h^0} = 115$  GeV,  $|X_t|/m_{\tilde{t}_2} = 0.3$  and the right panel a pessimistic case with  $m_{h^0} = 120$  GeV,  $|X_t|/m_{\tilde{t}_2} = 0.5$ . The range that can lead to electroweak-scale baryogenesis in the MSSM includes roughly  $235 \text{ GeV} < m_{\eta_{\tilde{t}}} < 270 \text{ GeV}$ .

#### IV. RESULTS FOR MODELS WITH ELECTROWEAK-SCALE BARYOGENESIS

Another motivation for a relatively light top squark is the possibility of achieving electroweak-scale baryogenesis in the MSSM [26]-[28]. The necessity of a strongly first-order phase transition to a meta-stable electroweak symmetry-breaking vacuum limits the allowed parameter space, requiring a mostly right-handed top squark with mass less than  $m_t$ . (For more details, see [26]-[28].) Here, I will consider a model framework proposed in [27], with an off-diagonal top-squark squared mass matrix element  $m_t X_t$  with  $0.3 \lesssim |X_t|/m_{\tilde{t}_2} \lesssim 0.5$ , and  $m_{\tilde{t}_2}$  very large (here 10 TeV),  $\tan\beta = 5$  to 10,  $m_{h^0}$  between 115 and 120 GeV, and all other superpartners except the LSP supposed to be sufficiently heavy that they do not mediate large contributions to the stoponium decay widths. Then the parameters with the most important impact on the stoponium decay widths are  $m_{h^0}$ ,  $m_{\tilde{t}_1}$ , and the top-squark mixing angle. The region of parameter space where electroweak-scale baryogenesis can work is roughly  $120 \text{ GeV} < m_{\tilde{t}_1} < 135 \text{ GeV}$  [28], but I will consider a wider range consistent with a meta-stable vacuum and the Higgs mass constraint from LEP2 [27].

In fig. 8, I show the relevant branching ratios for stoponium decay in a relatively optimistic case with  $m_{h^0} = 120$  GeV and  $|X_t|/m_{\tilde{t}_2} = 0.3$  (left panel), and a pessimistic case with  $m_{h^0} = 115$  GeV and  $|X_t|/m_{\tilde{t}_2} = 0.5$  (right panel). In both cases,  $\tan\beta = 10$ . Unfortunately, the branching ratio for the decay  $\eta_{\tilde{t}} \rightarrow h^0h^0$  is seen to be quite large above threshold [9, 13], due to a small denominator (coming from the top-squark propagator) in the last term in eq. (A.4). The  $\text{BR}(\eta_{\tilde{t}} \rightarrow h^0h^0)$  decreases as one moves to higher stoponium masses. I have made the optimistic but not unreasonable assumption that the other neutral Higgs boson  $H^0$  is sufficiently heavy that the decay  $\eta_{\tilde{t}} \rightarrow b\bar{b}$  is not near resonance and can be neglected. I have also optimistically assumed that the LSP is close enough in mass to  $\tilde{t}_1$  so that  $\eta_{\tilde{t}} \rightarrow \tilde{N}_1\tilde{N}_1$  is unimportant due to kinematic suppression.

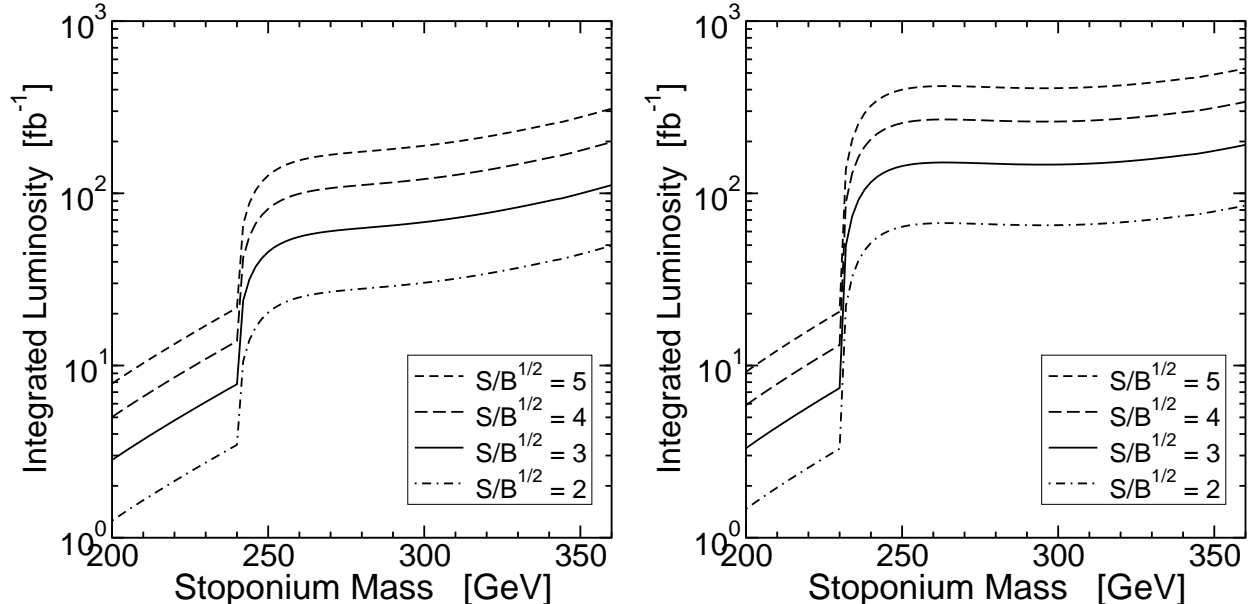


FIG. 9: Total integrated luminosity yielding an expected  $S/\sqrt{B} = 2, 3, 4, 5$  for  $M_{\gamma\gamma}$  in a bin with  $|M_{\gamma\gamma} - m_{\eta_{\tilde{t}}}| < 0.02m_{\eta_{\tilde{t}}}$ , as a function of the stoponium mass  $m_{\eta_{\tilde{t}}}$ , for  $pp$  collisions at  $\sqrt{s} = 14$  TeV, for the two model lines depicted in fig. 8. The range that can lead to electroweak-scale baryogenesis in the MSSM includes roughly  $235 \text{ GeV} < m_{\eta_{\tilde{t}}} < 270 \text{ GeV}$ .

The existing collider lower limits on  $m_{\tilde{t}_1}$  from the Tevatron and LEP2 do not constrain the top squark when  $m_{\tilde{t}_1} - m_{\tilde{N}_1}$  is small, because of the softness of the charm jets from the decay. Obtaining a thermal dark matter density in agreement with WMAP from stop-neutralino co-annihilations in these models requires  $m_{\tilde{t}_1} - m_{\tilde{N}_1} \gtrsim 20 \text{ GeV}$ , but a smaller mass difference is still allowed, since it would just mean that the dark matter is something else, for example axions, or LSPs arising from a non-thermal source.

Despite the large branching ratio to  $h^0 h^0$ , there are still good prospects for stoponium detection at the LHC in these models, because the stoponium mass is necessarily not too large. This can be seen in fig. 9, which depicts the required luminosity for detection at various expected significances, i.e. the results of fig. 4 divided by  $\text{BR}(\eta_{\tilde{t}} \rightarrow gg)^2$ . In the most optimistic case, a clear observation of stoponium could be possible with less than  $100 \text{ fb}^{-1}$  over a large range of stoponium masses including the range that can accommodate electroweak-scale baryogenesis. If the decay  $\eta_{\tilde{t}} \rightarrow h^0 h^0$  is kinematically forbidden, an observation could even be made with less than  $10 \text{ fb}^{-1}$ .

The detection of direct open light top squark production will probably be quite difficult at the LHC, especially if the  $m_{\tilde{t}_1} - m_{\tilde{N}_1}$  mass difference is very small, because then the charm jets from  $\tilde{t}_1 \rightarrow c\tilde{N}_1$  will be very soft. Most top squarks will likely come from gluino pair production followed by the decay  $\tilde{g} \rightarrow t\tilde{t}_1$ . The Majorana nature of the gluino implies that half of the resulting events will have like-charge top quarks and soft charm jets. This was found to be a viable signal in [64], and endpoint analyses will allow the determination of relations between the gluino, lighter stop, and LSP masses. A relatively precise measurement of  $m_{\eta_{\tilde{t}}}$  would clearly be very helpful in pinning down the masses of all three particles.

## V. OUTLOOK

In this paper, I have examined prospects for observing stoponium at the LHC in the process  $pp \rightarrow \eta_{\bar{t}} \rightarrow \gamma\gamma$ , as first suggested by Drees and Nojiri in [8, 9]. As illustrated in two distinct motivated scenarios, this search will likely be a long-term project, requiring good precision in the electromagnetic calorimetry and high integrated luminosity. For a positive detection with  $100 \text{ fb}^{-1}$  or less, it is estimated to be probably necessary (but certainly not sufficient) that the stoponium mass is less than about 500 GeV, which happens to be in the middle of the range preferred by compressed supersymmetry models of the type discussed in refs. [23, 24]. If the stoponium mass is less than 300 GeV, detection might even be possible with  $10 \text{ fb}^{-1}$  or less. My estimates of the detectability for the idealized case of models for which  $\text{BR}(\eta_{\bar{t}} \rightarrow gg) \approx 1$  are somewhat more pessimistic than in [9], but there is a clear opportunity if Nature is kind.

It would be useful to understand the higher-order corrections to stoponium production and decay, which might well have a large impact on the viability of the signal. Because these higher-order corrections are lacking for the signal, I have not included them for the background either, but they are likely to be substantial in both cases. In practice, the background will be obtainable from data using a sideband analysis. There is also an unknown, but possibly large, benefit from production of the excited states of stoponium adding to the signal.

An important remaining question is how accurately the observation of stoponium can determine the lighter top-squark mass, and from it other superpartner masses. The answer is quite sensitive to unknowns, including the true size of the backgrounds, the experimental mass resolution and systematic errors for diphotons, as well as an estimate of theoretical errors in the binding energies and wavefunctions for stoponium bound states. However, it seems clear that the observation of stoponium would present a unique opportunity to gain precise information about the superpartner masses, and a key ingredient in deciphering the mechanism behind supersymmetry breaking.

### Appendix: Stoponium partial decay widths

In this Appendix, I collect the results for the scalar stoponium annihilation decay widths. I agree with the results of ref. [9], except for the  $gg$  and  $\gamma\gamma$  widths; equations (A.1) and (A.2) of that reference should each be multiplied by a factor of 1/2 on the right side. (This is on top of, and distinct from, the factor of 1/2 for identical particles which is correctly included in equation (5) of ref. [9].) For these two widths, I agree with refs. [11] and [65]. Also, I have generalized ref. [9] slightly, by including the effects of sbottom mixing and possible CP violating phases. I use a convention in which chargino and neutralino masses are always real and positive. All equations below use couplings and other notations and conventions as given in detail in the second sections of the two papers in ref. [66], which will not be repeated here for the sake of brevity.

The general form for stoponium annihilation decay widths is

$$\Gamma(\eta_{\bar{t}} \rightarrow AB) = \frac{3}{32\pi^2(1 + \delta_{AB})} \lambda^{1/2}(1, m_A^2/m_{\eta_{\bar{t}}}^2, m_B^2/m_{\eta_{\bar{t}}}^2) \frac{|R(0)|^2}{m_{\eta_{\bar{t}}}^2} \sum |\mathcal{M}|^2, \quad (\text{A.1})$$

for  $AB = gg, \gamma\gamma, ZZ, h^0 h^0, Z\gamma, W^+W^-, t\bar{t}, b\bar{b}, \tilde{N}_i \tilde{N}_j$ , with  $\delta_{AB} = 1$  for the first four cases and the last case when  $i = j$ , and  $\delta_{AB} = 0$  in the others. Here  $\lambda(x, y, z) = x^2 + y^2 + z^2 - 2xy - 2xz - 2yz$ ,

and  $R(0)$  is the wavefunction at the origin, for which I use the  $\Lambda_{\overline{\text{MS}}}^{(4)} = 300 \text{ MeV}$  parameterization from Table A.1 of ref. [29] in numerical work; see eq. (2.3) of the present paper. It remains to give the spin-summed squared matrix element,  $\sum |\mathcal{M}|^2$ .

For the gluon-gluon and photon-photon final states, the results are independent of soft supersymmetry-breaking parameters, by gauge invariance:

$$\sum |\mathcal{M}(\eta_{\tilde{t}} \rightarrow gg)|^2 = \frac{16}{9} g_3^4 \quad (\text{A.2})$$

$$\sum |\mathcal{M}(\eta_{\tilde{t}} \rightarrow \gamma\gamma)|^2 = 8q_t^4 e^4 \quad (\text{A.3})$$

where  $q_t = 2/3$ . For the  $h^0 h^0$  final state,

$$|\mathcal{M}(\eta_{\tilde{t}} \rightarrow h^0 h^0)|^2 = \left( \lambda_{h^0 h^0 \tilde{t}_1 \tilde{t}_1^*} + \sum_{\phi^0 = h^0, H^0} \frac{\lambda_{\phi^0 \tilde{t}_1 \tilde{t}_1^*} \lambda_{h^0 h^0 \phi^0}}{4m_{\tilde{t}_1}^2 - m_{\phi^0}^2} - \sum_{j=1,2} \frac{2|\lambda_{h^0 \tilde{t}_1 \tilde{t}_j^*}|^2}{m_{\tilde{t}_1}^2 + m_{\tilde{t}_j}^2 - m_{h^0}^2} \right)^2. \quad (\text{A.4})$$

For the  $ZZ$  and  $W^+ W^-$  final states,

$$\sum |\mathcal{M}(\eta_{\tilde{t}} \rightarrow ZZ)|^2 = 2(a_{ZZ}^T)^2 + (a_{ZZ}^L)^2, \quad (\text{A.5})$$

$$\sum |\mathcal{M}(\eta_{\tilde{t}} \rightarrow W^+ W^-)|^2 = 2(a_{WW}^T)^2 + (a_{WW}^L)^2, \quad (\text{A.6})$$

where

$$a_{ZZ}^T = \frac{2}{g^2 + g'^2} \left[ \left( \frac{g^2}{2} - \frac{g'^2}{6} \right)^2 |L_{\tilde{t}_1}|^2 + \frac{4g'^4}{9} |R_{\tilde{t}_1}|^2 \right] + \sum_{\phi^0 = h^0, H^0} \frac{\lambda_{\phi^0 \tilde{t}_1 \tilde{t}_1^*} g_{ZZ\phi^0}}{4m_{\tilde{t}_1}^2 - m_{\phi^0}^2}, \quad (\text{A.7})$$

$$a_{ZZ}^L = (1 - 2m_{\tilde{t}_1}^2/m_Z^2) a_{ZZ}^T + \sum_{j=1,2} \frac{8}{g^2 + g'^2} \left| \left( \frac{g^2}{2} - \frac{g'^2}{6} \right) L_{\tilde{t}_1} L_{\tilde{t}_j}^* - \frac{2g'^2}{3} R_{\tilde{t}_1} R_{\tilde{t}_j}^* \right|^2 \frac{m_{\tilde{t}_1}^4/m_Z^2 - m_{\tilde{t}_1}^2}{m_{\tilde{t}_1}^2 + m_{\tilde{t}_j}^2 - m_Z^2}, \quad (\text{A.8})$$

$$a_{WW}^T = \frac{g^2}{2} |L_{\tilde{t}_1}|^2 + \sum_{\phi^0 = h^0, H^0} \frac{\lambda_{\phi^0 \tilde{t}_1 \tilde{t}_1^*} g_{WW\phi^0}}{4m_{\tilde{t}_1}^2 - m_{\phi^0}^2}, \quad (\text{A.9})$$

$$a_{WW}^L = (1 - 2m_{\tilde{t}_1}^2/m_W^2) a_{WW}^T + \sum_{j=1,2} 2g^2 |L_{\tilde{t}_1} L_{\tilde{b}_j}|^2 \frac{m_{\tilde{t}_1}^4/m_W^2 - m_{\tilde{t}_1}^2}{m_{\tilde{t}_1}^2 + m_{\tilde{b}_j}^2 - m_W^2}. \quad (\text{A.10})$$

For the  $Z\gamma$  final state,

$$\sum |\mathcal{M}(\eta_{\tilde{t}} \rightarrow Z\gamma)|^2 = 2q_t^2 e^2 (g^2 + g'^2) (|L_{\tilde{t}_1}|^2 - 4s_W^2/3)^2. \quad (\text{A.11})$$

The top-quark and bottom-quark final states have:

$$\sum |\mathcal{M}(\eta_{\tilde{t}} \rightarrow t\bar{t})|^2 = 6(m_{\tilde{t}_1}^2 - m_t^2) (2\text{Re}[a_{t\bar{t}}] - m_t b_{t\bar{t}})^2 + 24m_{\tilde{t}_1}^2 (\text{Im}[a_{t\bar{t}}])^2, \quad (\text{A.12})$$

$$\sum |\mathcal{M}(\eta_{\tilde{t}} \rightarrow b\bar{b})|^2 = 6(m_{\tilde{t}_1}^2 - m_b^2) (2\text{Re}[a_{b\bar{b}}] - m_b b_{b\bar{b}})^2 + 24m_{\tilde{t}_1}^2 (\text{Im}[a_{b\bar{b}}])^2, \quad (\text{A.13})$$

where

$$a_{t\tilde{t}} = \frac{(8g_3^2/9)m_{\tilde{g}}L_{\tilde{t}_1}^*R_{\tilde{t}_1}}{m_{\tilde{t}_1}^2 + m_{\tilde{g}}^2 - m_t^2} + \frac{y_t}{\sqrt{2}} \sum_{\phi^0=h^0,H^0,A^0} \frac{\lambda_{\phi^0\tilde{t}_1\tilde{t}_1^*}k_{u\phi^0}}{4m_{\tilde{t}_1}^2 - m_{\phi^0}^2} - \frac{1}{3} \sum_{j=1}^4 \frac{m_{\tilde{N}_j}Y_{t\tilde{N}_j\tilde{t}_1^*}Y_{\tilde{t}\tilde{N}_j\tilde{t}_1}}{m_{\tilde{t}_1}^2 + m_{\tilde{N}_j}^2 - m_t^2}, \quad (\text{A.14})$$

$$b_{t\tilde{t}} = \frac{8g_3^2/9}{m_{\tilde{t}_1}^2 + m_{\tilde{g}}^2 - m_t^2} + \frac{1}{3} \sum_{j=1}^4 \frac{|Y_{t\tilde{N}_j\tilde{t}_1^*}|^2 + |Y_{\tilde{t}\tilde{N}_j\tilde{t}_1}|^2}{m_{\tilde{t}_1}^2 + m_{\tilde{N}_j}^2 - m_t^2}, \quad (\text{A.15})$$

$$a_{b\tilde{b}} = \frac{y_b}{\sqrt{2}} \sum_{\phi^0=h^0,H^0,A^0} \frac{\lambda_{\phi^0\tilde{t}_1\tilde{t}_1^*}k_{d\phi^0}}{4m_{\tilde{t}_1}^2 - m_{\phi^0}^2} - \frac{1}{3} \sum_{j=1}^2 \frac{m_{\tilde{C}_j}Y_{b\tilde{C}_j\tilde{t}_1^*}Y_{\tilde{b}\tilde{C}_j\tilde{t}_1}}{m_{\tilde{t}_1}^2 + m_{\tilde{C}_j}^2 - m_b^2}, \quad (\text{A.16})$$

$$b_{b\tilde{b}} = \frac{1}{3} \sum_{j=1}^2 \frac{|Y_{b\tilde{C}_j\tilde{t}_1^*}|^2 + |Y_{\tilde{b}\tilde{C}_j\tilde{t}_1}|^2}{m_{\tilde{t}_1}^2 + m_{\tilde{C}_j}^2 - m_b^2}. \quad (\text{A.17})$$

Finally, the final state with neutralinos has:

$$\begin{aligned} \sum |\mathcal{M}(\eta_{\tilde{t}} \rightarrow \tilde{N}_j\tilde{N}_k)|^2 &= |a_{\tilde{N}_j\tilde{N}_k}|^2(8m_{\tilde{t}_1}^2 - 2m_{\tilde{N}_j}^2 - 2m_{\tilde{N}_k}^2) - 4m_{\tilde{N}_j}m_{\tilde{N}_k}\text{Re}[(a_{\tilde{N}_j\tilde{N}_k})^2] \\ &\quad + |b_{\tilde{N}_j\tilde{N}_k}|^2 \left[ 2m_{\tilde{t}_1}^2(m_{\tilde{N}_j}^2 + m_{\tilde{N}_k}^2) - 3m_{\tilde{N}_j}^2m_{\tilde{N}_k}^2 - (m_{\tilde{N}_j}^4 + m_{\tilde{N}_k}^4)/2 \right] \\ &\quad + \text{Re}[(b_{\tilde{N}_j\tilde{N}_k})^2]m_{\tilde{N}_j}m_{\tilde{N}_k}(4m_{\tilde{t}_1}^2 - 2m_{\tilde{N}_j}^2 - 2m_{\tilde{N}_k}^2) \\ &\quad + 2\text{Re}[a_{\tilde{N}_j\tilde{N}_k}b_{\tilde{N}_j\tilde{N}_k}]m_{\tilde{N}_j}(4m_{\tilde{t}_1}^2 - m_{\tilde{N}_j}^2 - 3m_{\tilde{N}_k}^2) \\ &\quad + 2\text{Re}[a_{\tilde{N}_j\tilde{N}_k}b_{\tilde{N}_j\tilde{N}_k}^*]m_{\tilde{N}_k}(4m_{\tilde{t}_1}^2 - 3m_{\tilde{N}_j}^2 - m_{\tilde{N}_k}^2), \end{aligned} \quad (\text{A.18})$$

where

$$a_{\tilde{N}_j\tilde{N}_k} = \frac{m_t(Y_{t\tilde{N}_j\tilde{t}_1^*}Y_{\tilde{t}\tilde{N}_k\tilde{t}_1} + Y_{\tilde{t}\tilde{N}_j\tilde{t}_1}Y_{t\tilde{N}_k\tilde{t}_1^*})}{m_{\tilde{t}_1}^2 + m_t^2 - (m_{\tilde{N}_j}^2 + m_{\tilde{N}_k}^2)/2} - \sum_{\phi^0=h^0,H^0,A^0} \frac{\lambda_{\phi^0\tilde{t}_1\tilde{t}_1^*}Y_{\tilde{N}_j\tilde{N}_k\phi^0}}{4m_{\tilde{t}_1}^2 - m_{\phi^0}^2}, \quad (\text{A.19})$$

$$b_{\tilde{N}_j\tilde{N}_k} = \frac{Y_{t\tilde{N}_j\tilde{t}_1^*}Y_{\tilde{t}\tilde{N}_k\tilde{t}_1^*}^* + Y_{\tilde{t}\tilde{N}_j\tilde{t}_1}^*Y_{\tilde{t}\tilde{N}_k\tilde{t}_1}}{m_{\tilde{t}_1}^2 + m_t^2 - (m_{\tilde{N}_j}^2 + m_{\tilde{N}_k}^2)/2}. \quad (\text{A.20})$$

If there are no CP-violating phases, then  $a_{\tilde{N}_j\tilde{N}_k}$  and  $b_{\tilde{N}_j\tilde{N}_k}$  are real, and eq. (A.18) simplifies to:

$$\sum |\mathcal{M}(\eta_{\tilde{t}} \rightarrow \tilde{N}_j\tilde{N}_k)|^2 = 2[4m_{\tilde{t}_1}^2 - (m_{\tilde{N}_j} + m_{\tilde{N}_k})^2][a_{\tilde{N}_j\tilde{N}_k} + (m_{\tilde{N}_j} + m_{\tilde{N}_k})b_{\tilde{N}_j\tilde{N}_k}/2]^2. \quad (\text{A.21})$$

*Acknowledgments:* I thank Tulika Bose, Gustaaf Brooijmans, Manuel Drees, Germano Nardini, Mihoko Nojiri and Carlos Wagner for helpful communications. This work was supported in part by the National Science Foundation grant number PHY-0456635.

---

[1] M. Drees, R. Godbole and P. Roy, ‘‘Theory and phenomenology of sparticles: An account of four-dimensional N=1 supersymmetry in high energy physics,’’ *World Scientific (2004)*.



- [2] H. Baer and X. Tata, “Weak scale supersymmetry: From superfields to scattering events,” *Cambridge University Press* (2006).
- [3] S.P. Martin, “A supersymmetry primer,” [hep-ph/9709356] (version 4, June 2006).
- [4] The ATLAS collaboration, “ATLAS Detector and physics performance technical design report”, Volume 2. CERN-LHCC-99-15, ATLAS-TDR-15, May 1999.
- [5] The CMS collaboration, “CMS Physics Technical Design Report”, Volume 1, Detector Performance and Software. CERN-LHCC-2006-001, CMS TDR 8.1, February 2006.
- [6] K. i. Hikasa and M. Kobayashi, *Phys. Rev. D* **36**, 724 (1987).
- [7] W. Porod and T. Wohrman, *Phys. Rev. D* **55**, 2907 (1997) [Erratum-ibid. *D* **67**, 059902 (2003)] [hep-ph/9608472].
- [8] M. Drees and M.M. Nojiri, *Phys. Rev. Lett.* **72**, 2324 (1994) [hep-ph/9310209].
- [9] M. Drees and M.M. Nojiri, *Phys. Rev. D* **49**, 4595 (1994) [hep-ph/9312213].
- [10] C.R. Nappi, *Phys. Rev. D* **25**, 84 (1982).
- [11] P. Moxhay and R.W. Robinett, *Phys. Rev. D* **32**, 300 (1985).
- [12] M.J. Herrero, A. Mendez and T.G. Rizzo, *Phys. Lett. B* **200**, 205 (1988).
- [13] V.D. Barger and W.Y. Keung, *Phys. Lett. B* **211**, 355 (1988).
- [14] H. Inazawa and T. Morii, *Phys. Rev. Lett.* **70**, 2992 (1993).
- [15] D.N. Spergel *et al.* [WMAP Collaboration], “Wilkinson Microwave Anisotropy Probe (WMAP) three year results: Implications for cosmology,” [astro-ph/0603449].
- [16] M. Tegmark *et al.* [SDSS Collaboration], *Phys. Rev. D* **69**, 103501 (2004) [astro-ph/0310723].
- [17] W.M. Yao *et al.* [Particle Data Group], “Review of particle physics,” *J. Phys. G* **33**, 1 (2006).
- [18] C. Boehm, A. Djouadi and M. Drees, *Phys. Rev. D* **62**, 035012 (2000) [hep-ph/9911496];
- [19] J.R. Ellis, K.A. Olive and Y. Santoso, *Astropart. Phys.* **18**, 395 (2003) [hep-ph/0112113];
- [20] J. Edsjo, M. Schelke, P. Ullio and P. Gondolo, *JCAP* **0304**, 001 (2003) [hep-ph/0301106], J. Edsjo, M. Schelke and P. Ullio, *JCAP* **0409**, 004 (2004) [astro-ph/0405414].
- [21] C. Balazs, M. Carena and C.E.M. Wagner, *Phys. Rev. D* **70**, 015007 (2004) [hep-ph/0403224].
- [22] G. Belanger, F. Boudjema, S. Kraml, A. Pukhov and A. Semenov, *Phys. Rev. D* **73**, 115007 (2006) [hep-ph/0604150].
- [23] S.P. Martin, *Phys. Rev. D* **75**, 115005 (2007) [hep-ph/0703097].
- [24] S.P. Martin, *Phys. Rev. D* **76**, 095005 (2007) [hep-ph/0707.2812].
- [25] G.L. Kane and S.F. King, *Phys. Lett. B* **451**, 113 (1999) [hep-ph/9810374], M. Bastero-Gil, G.L. Kane and S.F. King, *Phys. Lett. B* **474**, 103 (2000) [hep-ph/9910506].
- [26] J.R. Espinosa, M. Quiros and F. Zwirner, *Phys. Lett. B* **307**, 106 (1993) [hep-ph/9303317], M.S. Carena, M. Quiros and C.E.M. Wagner, *Phys. Lett. B* **380**, 81 (1996) [hep-ph/9603420], *Nucl. Phys. B* **524**, 3 (1998) [hep-ph/9710401], J.R. Espinosa, *Nucl. Phys. B* **475**, 273 (1996) [hep-ph/9604320], D. Bodeker, P. John, M. Laine and M. G. Schmidt, *Nucl. Phys. B* **497**, 387 (1997) [hep-ph/9612364], M.S. Carena, M. Quiros, A. Riotto, I. Vilja and C.E.M. Wagner, *Nucl. Phys. B* **503**, 387 (1997) [hep-ph/9702409], J.M. Cline, M. Joyce and K. Kainulainen, *Phys. Lett. B* **417**, 79 (1998) [Erratum-ibid. *B* **448**, 321 (1999)] [hep-ph/9708393], *JHEP* **0007**, 018 (2000) [hep-ph/0006119], J.M. Cline and G.D. Moore, *Phys. Rev. Lett.* **81**, 3315 (1998) [hep-ph/9806354], M.S. Carena, M. Quiros, M. Seco and C.E.M. Wagner, *Nucl. Phys. B* **650**, 24 (2003) [hep-ph/0208043].
- [27] C. Balazs, M.S. Carena and C.E.M. Wagner, *Phys. Rev. D* **70**, 015007 (2004) [hep-ph/0403224]. C. Balazs, M.S. Carena, A. Menon, D.E. Morrissey and C.E.M. Wagner, *Phys. Rev. D* **71**, 075002 (2005) [hep-ph/0412264].
- [28] M.S. Carena, G. Nardini, M. Quiros, and C.E.M. Wagner, to appear.
- [29] K. Hagiwara, K. Kato, A.D. Martin and C.K. Ng, *Nucl. Phys. B* **344**, 1 (1990).
- [30] V.D. Barger *et al.*, *Phys. Rev. D* **35**, 3366 (1987) [Erratum-ibid. *D* **38**, 1632 (1988)].
- [31] H.L. Lai *et al.* [CTEQ Collaboration], *Eur. Phys. J. C* **12**, 375 (2000) [hep-ph/9903282].
- [32] R. Karplus and M. Neuman, *Phys. Rev.* **83**, 776 (1951).
- [33] B. De Tollis, *Nuovo Cim.* **32**, 757 (1964).
- [34] V. Costantini, B. De Tollis and G. Pistoni, *Nuovo Cim. A* **2**, 733 (1971).
- [35] D.A. Dicus and S.S.D. Willenbrock, *Phys. Rev. D* **37**, 1801 (1988).

- [36] C. Balazs, P. Nadolsky, C. Schmidt and C.P. Yuan, *Phys. Lett. B* **489**, 157 (2000) [hep-ph/9905551].
- [37] T. Binoth, J.P. Guillet, E. Pilon and M. Werlen, *Eur. Phys. J. C* **16**, 311 (2000) [hep-ph/9911340].
- [38] Z. Bern, A. De Freitas and L.J. Dixon, *JHEP* **0109**, 037 (2001) [hep-ph/0109078], Z. Bern, L.J. Dixon and C. Schmidt, *Phys. Rev. D* **66**, 074018 (2002) [hep-ph/0206194].
- [39] C. Balazs, E.L. Berger, P.M. Nadolsky and C.P. Yuan, *Phys. Lett. B* **637**, 235 (2006) [hep-ph/0603037], *Phys. Rev. D* **76**, 013009 (2007) [hep-ph/0704.0001].
- [40] M.-C. Lemaire, V.A. Litvin and H. Newman, “Search for Randall-Sundrum excitations of gravitons decaying into two photons for CMS at LHC,” CERN-CMS-NOTE-2006-051.
- [41] G. Belanger, F. Boudjema, A. Pukhov and A. Semenov, “micrOMEGAs2.0: A program to calculate the relic density of dark matter in a generic model,” *Comput. Phys. Commun.* **176**, 367 (2007) [hep-ph/0607059], *Comput. Phys. Commun.* **174**, 577 (2006) [hep-ph/0405253], *Comput. Phys. Commun.* **149**, 103 (2002) [hep-ph/0112278].
- [42] P. Gondolo, J. Edsjö, P. Ullio, L. Bergstrom, M. Schelke and E.A. Baltz, “DarkSUSY: Computing supersymmetric dark matter properties numerically,” *JCAP* **0407**, 008 (2004) [astro-ph/0406204];
- [43] B.C. Allanach, “SOFTSUSY: A C++ program for calculating supersymmetric spectra,” *Comput. Phys. Commun.* **143**, 305 (2002) [hep-ph/0104145].
- [44] A. Djouadi, J.L. Kneur and G. Moultaka, “SuSpect: A Fortran code for the supersymmetric and Higgs particle spectrum in the MSSM,” [hep-ph/0211331].
- [45] F.E. Paige, S.D. Protopopescu, H. Baer and X. Tata, “ISAJET 7.69: A Monte Carlo event generator for p p, anti-p p, and e+ e- reactions,” [hep-ph/0312045].
- [46] H. Baer, A. Box, E.K. Park and X. Tata, *JHEP* **0708**, 060 (2007) [hep-ph/0707.0618].
- [47] A. Corsetti and P. Nath, *Phys. Rev. D* **64**, 125010 (2001) [hep-ph/0003186], *Phys. Rev. D* **66**, 035003 (2002) [hep-ph/0201001].
- [48] A. Birkedal-Hansen and B.D. Nelson, *Phys. Rev. D* **64**, 015008 (2001) [hep-ph/0102075], *Phys. Rev. D* **67**, 095006 (2003) [hep-ph/0211071].
- [49] H. Baer et al, *JHEP* **0205**, 061 (2002) [hep-ph/0204108].
- [50] V. Bertin, E. Nezri and J. Orloff, *JHEP* **0302**, 046 (2003) [hep-ph/0210034].
- [51] U. Chattopadhyay and D.P. Roy, *Phys. Rev. D* **68**, 033010 (2003) [hep-ph/0304108].
- [52] D.G. Cerdeño and C. Muñoz, *JHEP* **0410**, 015 (2004) [hep-ph/0405057].
- [53] G. Belanger, F. Boudjema, A. Cottrant, A. Pukhov and A. Semenov, *Nucl. Phys. B* **706**, 411 (2005) [hep-ph/0407218], *Czech. J. Phys.* **55**, B205 (2005) [hep-ph/0412309].
- [54] Y. Mambrini and E. Nezri, *Eur. Phys. J. C* **50**, 949 (2007) [hep-ph/0507263].
- [55] S.F. King and J.P. Roberts, *JHEP* **0609**, 036 (2006) [hep-ph/0603095]; *JHEP* **0701**, 024 (2007) [hep-ph/0608135].
- [56] H. Baer, A. Mustafayev, E.K. Park, S. Profumo and X. Tata, *JHEP* **0604**, 041 (2006) [hep-ph/0603197], H. Baer, A. Mustafayev, S. Profumo and X. Tata, *Phys. Rev. D* **75**, 035004 (2007) [hep-ph/0610154].
- [57] N. Arkani-Hamed, A. Delgado and G.F. Giudice, *Nucl. Phys. B* **741**, 108 (2006) [hep-ph/0601041].
- [58] A. Falkowski, O. Lebedev and Y. Mambrini, *JHEP* **0511**, 034 (2005) [hep-ph/0507110].
- [59] J.R. Ellis, K.A. Olive and P. Sandick, *Phys. Lett. B* **642**, 389 (2006) [hep-ph/0607002], *JHEP* **0706**, 079 (2007) [hep-ph/0704.3446].
- [60] H. Baer, E.K. Park, X. Tata and T.T. Wang, *JHEP* **0608**, 041 (2006) [hep-ph/0604253]; *JHEP* **0706**, 033 (2007) [hep-ph/0703024].
- [61] K.J. Bae, R. Dermisek, H.D. Kim and I.W. Kim, *JCAP* **0708**, 014 (2007) [hep-ph/0702041].
- [62] S.F. King, J.P. Roberts and D.P. Roy, *JHEP* **0710**, 106 (2007) [hep-ph/0705.4219].
- [63] H. Baer, A. Mustafayev, H. Summy and X. Tata, *JHEP* **0710**, 088 (2007) [hep-ph/0708.4003].
- [64] S. Kraml and A.R. Raklev, *Phys. Rev. D* **73**, 075002 (2006) [hep-ph/0512284].
- [65] D.S. Gorbunov and V.A. Ilyin, *JHEP* **0011**, 011 (2000) [hep-ph/0004092].
- [66] S.P. Martin, *Phys. Rev. D* **66**, 096001 (2002) [hep-ph/0206136], *Phys. Rev. D* **71**, 016012 (2005) [hep-ph/0405022].